



HAL
open science

Comparing satellite and surface rainfall products over West Africa at meteorologically relevant scales during the AMMA campaign using error estimates

Remy Roca, Philippe Chambon, Isabelle Jobard, Pierre-Emmanuel Kirstetter, Marielle Gosset, Jean-Claude Bergès

► To cite this version:

Remy Roca, Philippe Chambon, Isabelle Jobard, Pierre-Emmanuel Kirstetter, Marielle Gosset, et al.. Comparing satellite and surface rainfall products over West Africa at meteorologically relevant scales during the AMMA campaign using error estimates. *Journal of Applied Meteorology and Climatology*, 2010, 49 (4), pp.715-731. 10.1175/2009JAMC2318.1 . hal-00438715

HAL Id: hal-00438715

<https://hal.science/hal-00438715>

Submitted on 22 Nov 2020

HAL is a multi-disciplinary open access archive for the deposit and dissemination of scientific research documents, whether they are published or not. The documents may come from teaching and research institutions in France or abroad, or from public or private research centers.

L'archive ouverte pluridisciplinaire **HAL**, est destinée au dépôt et à la diffusion de documents scientifiques de niveau recherche, publiés ou non, émanant des établissements d'enseignement et de recherche français ou étrangers, des laboratoires publics ou privés.



Comparing Satellite and Surface Rainfall Products over West Africa at Meteorologically Relevant Scales during the AMMA Campaign Using Error Estimates

RÉMY ROCA

Laboratoire de Météorologie Dynamique, IPSL/CNRS, Paris, France

PHILIPPE CHAMBON AND ISABELLE JOBARD

Laboratoire de Météorologie Dynamique, IPSL/CNRS, Palaiseau, France

PIERRE-EMMANUEL KIRSTETTER

Laboratoire ATMOS, IPSL/CNRS, Vélizy, France

MARIELLE GOSSET

Laboratoire d'étude des Transferts en Hydrologie et Environnement, Grenoble, France

JEAN CLAUDE BERGÈS

PRODIG, Université Paris 1, Paris, France

(Manuscript received 9 June 2009, in final form 16 November 2009)

ABSTRACT

Monsoon rainfall is central to the climate of West Africa, and understanding its variability is a challenge for which satellite rainfall products could be well suited to contribute to. Their quality in this region has received less attention than elsewhere. The focus is set on the scales associated with atmospheric variability, and a meteorological benchmark is set up with ground-based observations from the African Monsoon Multidisciplinary Analysis (AMMA) program. The investigation is performed at various scales of accumulation using four gauge networks. The seasonal cycle is analyzed using 10-day-averaged products, the synoptic-scale variability is analyzed using daily means, and the diurnal cycle of rainfall is analyzed at the seasonal scale using a composite and at the diurnal scale using 3-hourly accumulations. A novel methodology is introduced that accounts for the errors associated with the areal-time rainfall averages. The errors from both satellite and ground rainfall data are computed using dedicated techniques that come down to an estimation of the sampling errors associated to these measurements. The results show that the new generation of combined infrared-microwave (IR-MW) satellite products is describing the rain variability similarly to ground measurements. At the 10-day scale, all products reveal high regional and seasonal skills. The day-to-day comparison indicates that some products perform better than others, whereas all of them exhibit high skills when the spectral band of African easterly waves is considered. The seasonal variability of the diurnal scale as well as its relative daily importance is only captured by some products. Plans for future extensive intercomparison exercises are briefly discussed.

1. Introduction

The West African monsoon (WAM) brings the main part of the yearly rainfall over West Africa, including

Sahel (Hastenrath 1991), and is at the heart of the water resources of this part of the continent (Conway et al. 2009). The functioning of the monsoon and of the rainfall variability has hence received a lot of attention, especially since the advent of a long-term drought over the Sahel in the 1970s to the 1990s (Le Barbé et al. 2002; Ali and Lebel 2008; Giannini et al. 2008a). Its future evolution is also of concern in the context of the global climate change (e.g., Giannini et al. 2008b). The need for

Corresponding author address: Dr. Rémy Roca, Laboratoire de Météorologie Dynamique, Tour 45-55, 3ème étage, Case Postale 99, 4 place Jussieu, 75252 Paris, CEDEX 05, France.
E-mail: roca@lmd.jussieu.fr

a deeper understanding and forecasting capability of the WAM prompted the community to devote a vast observational program over the region, the African Monsoon Multidisciplinary Analysis (AMMA; Redelsperger et al. 2006); the data from the AMMA campaign are used in this study.

The main feature of the seasonal march of the monsoon is the rapid onset occurring in late June and characterized by a northward jump of the ITCZ (Sultan and Janicot 2003) showing a strong modification of the rain regimes and synoptic-scale variability (Gu and Adler 2004). The day-to-day variability of rainfall alternates between active and inactive phases at the intraseasonal scale with modes at 10–25 days and around 40–50 days, respectively (Sultan et al. 2003). At shorter synoptic time scales, variability of the rainfall is also observed and linked to tropical wave dynamics (e.g., Gu et al. 2003; Mounier et al. 2007) and extratropical intrusions of dry air (Roca et al. 2005). The most documented mode of synoptic variability is associated with the African easterly waves (AEW) and was recently fully redocumented (Kiladis et al. 2006). These 3–5-day waves are modulating strongly the rainfall during the monsoon through their relationship to organized convective systems (Machado et al. 1993). Finally, as observed on most tropical continents, the diurnal cycle of insolation drives a significant portion of the overall meteorological variability over the WAM (e.g., Desbois et al. 1988). Redelsperger et al. (2002) systematically investigated the 1992 wet season in West Africa and detailed the previously mentioned various scales for that very year. They underscored that such a multiscale approach was an encouraging method to deepen our understanding of the interaction of the various processes occurring in the WAM. Hence, further understanding of the WAM requires in-depth analysis of this multiscale variability of rainfall.

Satellite observations are a powerful tool to cover these scales and to be used for these much needed meteorological investigations over the WAM where the pluviograph network is scarce. The recent generation of combined infrared (IR) and microwave (MW) products (Hsu et al. 1997; Herman et al. 1997; Huffman et al. 2001; Joyce et al. 2004; Ushio et al. 2009; Huffman et al. 2007; Levizzani et al. 2007; Bergès et al. 2010) especially fits very well to such endeavor, but their hard-to-tell ability to provide useful information is often underscored. Although a number of studies investigated the quality of these satellite estimates in various regions of the world [e.g., Negri et al. 1995; Ebert et al. 1996; Ebert and Manton 1998; Joyce et al. 2004; Huffman et al. 2007; Xie et al. 2007; Ebert et al. 2007; Zeweldi and Gebremichael 2009; Sapiiano and Arkin 2009; see also the International Precipitation Working Group (IPWG)

Web site, which is available online at <http://www.isac.cnr.it/~ipwg/IPWG.html>], few addressed the West African climate. These rare studies focused on accumulated time scales such as 10-day and monthly scales (Laurent et al. 1998; Nicholson et al. 2003a,b; Ali et al. 2005b; Lamptey 2008). Jobard et al. (2010) recently provided 10-day scale intercomparisons of 10 products using 3 yr of data over the Sahel. Their results indicate good enough agreements at this scale to conduct further investigation at shorter time scales in link with the meteorology of the region.

Here, we provide a comparison of a representative subset of IR–MW satellite and surface rainfall products over West Africa, at meteorologically relevant scales, during the AMMA campaign (2006 rainy season). Our aim is to validate (or not) the use of the satellite rainfall estimates for physical investigation of the monsoon. The 10-day scale before and after the onset, the daily scale over the full course of the monsoon, the 3–5-day spectral band before and after the onset, and the diurnal scale before and after the onset are documented as a meteorological benchmark to establish the usefulness of the satellite rain products. A dedicated statistical approach is proposed that relies on the use in the comparisons of the errors associated to the areal mean rainfall estimates for both gauges and satellite products. This novel methodology is applied at the previously mentioned scales over the WAM region and over three dedicated sites that were adequately instrumented during the AMMA campaign (Lebel et al. 2009, 2010).

The paper is organized as follows: First, ground-based and satellite data are both introduced along with their respective error budget in section 2. Section 3 quickly presents the statistical procedure, taking the errors into account, used for the comparison. Section 4 details the results of the confrontation for each scale of our meteorological benchmark. A summary and discussion are reported in section 5.

2. Data

a. Rationale

Over the mentioned range of scales, classical (without errors) evaluation techniques (for an insightful review, see Ebert 2007) fall short as the errors in both the gauges, and the satellite products can become significant and can corrupt the evaluation. For instance, the measurement errors significantly attenuate the observed correlation, making the observed correlation between two series weaker than if one does not account for the measurement errors. Kelly (2007) shows that, when the measurements errors make up to 50% of the variance on each series, the coefficient of correlation is reduced by roughly 50%. Such

an example calls for a careful handling of the errors in running the comparisons. The estimation of the errors in both the gauges and the satellite rainfall estimates is a complex task. It is therefore usually left aside by the investigators in intercomparison exercises (Ebert 2007). Such efforts have nevertheless been undertaken at different time and space scales for both satellite measurements over different parts of the world (e.g., Huffman 1997; Ali et al. 2005b) and gauge measurements (e.g., Lebel et al. 1987; Morrissey et al. 1995; Ali et al. 2005a; Grimes et al. 1999; Pardo-Igúzquiza et al. 2006; Teo and Grimes 2007). In short, the error budget of the satellite and gauges products can be written as

$$S^2 = S_{\text{calibration}}^2 + S_{\text{algorithm}}^2 + S_{\text{sampling}}^2, \quad (1)$$

where the calibration term is associated with systematic errors and relevant to the accuracy of the products. The algorithm term is associated with the intrinsic errors of the retrieval, and the sampling term refers purely to the error resulting from the discrete nature (in space or time) of observations; both terms are relevant to the accuracy and the precision of the products. It is difficult to separate both latter terms, because the precision and accuracy of retrievals depends on the scale of interest and hence the sampling term is sometimes considered as a mixture of the two (Huffman 1997).

Rainfall estimation by gauges is subject to a very low measurement error (e.g., Ciach and Krajewski 1999) because of the direct nature of this measurement. On the other hand, because of the punctual nature of gauge measurement, the sampling error when computing areal mean rainfall cannot be neglected. The algorithm-based errors can be assumed to be small compared to the sampling errors of the gauges (Habib et al. 2001), even if uncertainty can be significant at small rain rates and accumulation scales (Ciach 2003). Satellite products are not affected by a calibration uncertainty of a few Kelvin's for the geostationary IR and low earth orbit satellite (LEO) microwave brightness temperatures (Jobard and Desbois 1994; Viltard et al. 2006), and we hence neglect it in the error budget. The algorithm term is difficult to estimate and is usually considered to be small compared to the sampling uncertainty. Gebremichael and Krajewski (2005), based on previous studies, assumed that sampling errors indeed dominate the error budget of satellite products and proposed a parametric model of the sampling error distribution of rainfall depending on the mean rainfall from radar measurements from monthly down to daily scale over a variety of space scales. The error budget for both ground-based and satellite-based rain products hence finally reduces to

TABLE 1. Characteristics of the rain gauge networks.

Name	Localization	Area	Gauges
CILSS	10.0°–17.5°N, 17.5°W–22.5°E	4 000 000 km ²	570
Niamey	13.0°–14.2°N, 1.4°–3.0°E	25 000 km ²	54
Ouémé	9.0°–10.0°N, 1.5°–2.8°E	15 400 km ²	52
Dakar	14.4°–14.7°N, 16.9°–16.6°W	1200 km ²	21

$$S^2 \sim S_{\text{sampling}}^2. \quad (2)$$

The sampling term error computations are performed using two different approaches for the gauges and satellite rain estimates, even if the techniques are closely related to each other. Errors are evaluated for each areal-averaged estimate at various scales.

b. The ground-based rain products

1) RAIN GAUGE NETWORKS

Four rain gauge networks are used for this study. The characteristics of the areas and localization of the networks sites are presented in Table 1, and their gauge distributions are shown in Figs. 1 and 2. The Comité Permanent Inter-Etats de Lutte contre la Sécheresse dans le Sahel (CILSS) rain gauge network, spread over the Sahelian band (Fig. 1), included during the 2006 rainy season about 570 rain gauge stations and 75 synoptic stations of the Global Telecommunication System (GTS). The GTS stations are not used for this study because they are used in some of the satellite products. The daily rain data are aggregated at a 10-day time resolution for regional comparison with satellite estimations.

The three other networks cover smaller areas located in Niger, Benin and Senegal. The Benin and Niger networks are part of the AMMA Coupling the Tropical Atmosphere and the Hydrological Cycle (AMMA-CATCH) observing system (Lebel et al. 2009). The distribution of gauges of the network around Niamey was optimized (Lebel and Amani 1999) to obtain a good accuracy for rainfall estimation over the area at the rain event scale (typically a few hours); the number of tipping-bucket gauges was increased up to 54 for the AMMA enhanced observing period (EOP) in 2006. The upper Ouémé catchment in Benin was instrumented with 52 tipping-bucket gauges at stations that are evenly distributed on a surface of about 15 000 km². This configuration is suitable for the mesoscale analysis of the rainfall associated with tropical convective systems. Both the Ouémé and Niamey networks have a density of about 1 gauge per 200 km² over a 1° × 1° area. The Dakar network consisted of about 35 stations unevenly distributed over a 1° × 1° area (Jenkins et al. 2010, unpublished manuscript; Jenkins and Gaye 2010); only a subsample of the network

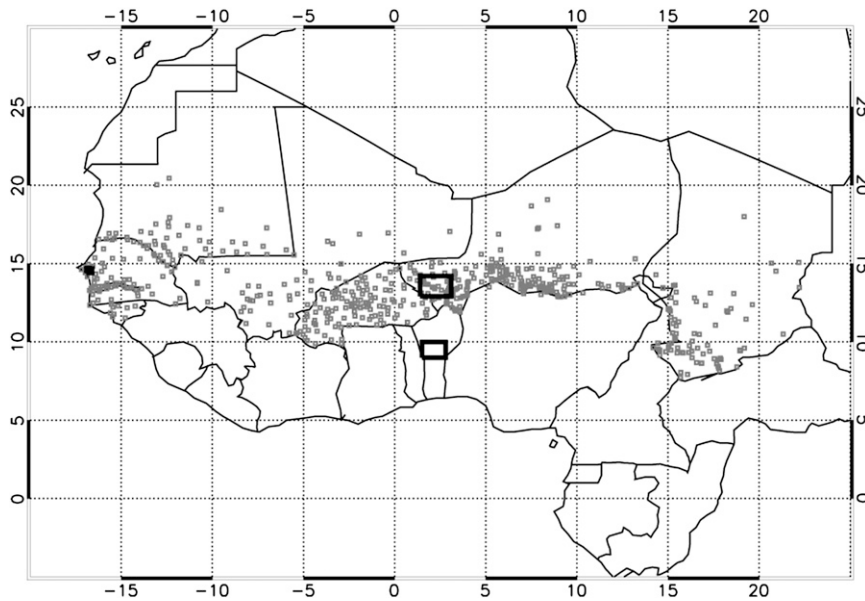


FIG. 1. CILSS area rain gauge network distribution (Ali et al. 2005a).

on a small, denser area ($0.3^\circ \times 0.3^\circ$) that includes 21 gauges (see Fig. 2c) available for two months (August–September 2006), a density of about 1 gauge per 50 km^2 . The gauge data from these three networks are computed at 3-h and daily time steps and also aggregated into mean seasonal diurnal cycle.

2) PRODUCTS AND ASSOCIATED ERROR COMPUTATION

Various techniques of rain gauge point value interpolation have been developed to estimate not only area-averaged ground rainfall accumulation but also the sampling errors associated to the interpolation of the point values over their surrounding spatial domain. Among those techniques, linear estimators are widespread

used interpolators, and their general expression for $R_{\text{ref}}(A, T)$ area rainfall estimate over a spatial domain A and a period of accumulation T is

$$R_{\text{ref}}(A, T) = \sum_{i=1}^{N_g} \lambda_i R_g(x_i, T), \quad (3)$$

where λ_i represents weights on the accumulations of the i th rain gauges $R_g(x_i, T)$ and N_g represents the total number of rain gauges available. Morrissey et al. (1995) detail the computation of an unweighted linear interpolation of rain gauge accumulations and compare sampling errors associated to various geometries of networks. Here, the ordinary block-kriging technique (Journal and Huijbregts 1978) is used to estimate area rainfall

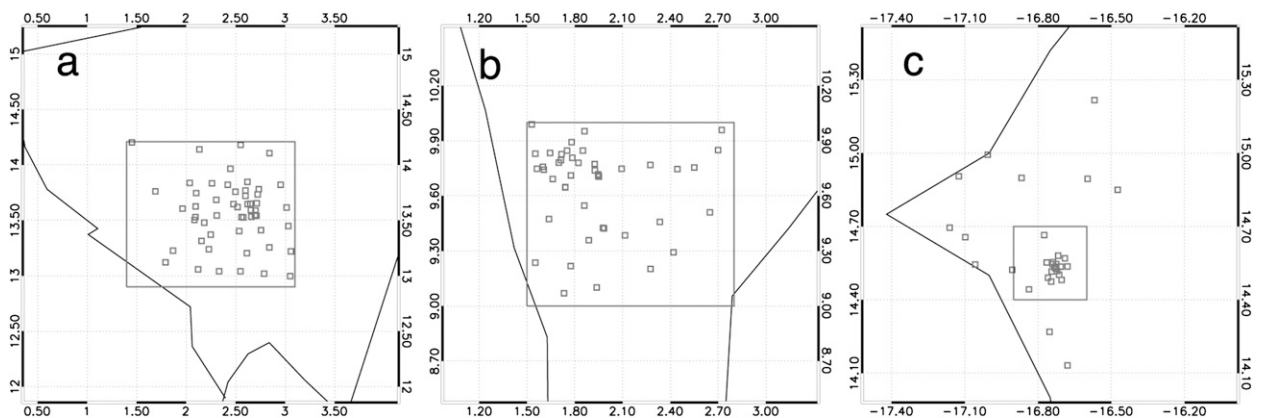


FIG. 2. Rain gauge distributions of the three dense networks of (a) Niamey, (b) Ouémé, and (c) Dakar. The squares represent the area selected for the kriging interpolation. Black lines are the borders of Niger, Benin and Senegal.

estimates and their respective sampling errors, first for 10-day accumulations over 1° grid boxes in the Sahel (Ali et al. 2005a) and then for daily and 3-hourly accumulations and for a 3-hourly seasonally cumulated diurnal cycle over the three sites of Niamey, Ouémé, and Dakar. By weighting the rain gauges individually, the characteristic of the kriging estimator is unbiased and the estimation variance is minimized (Lebel and Amani 1999). The kriging technique relies on a structure function of the rain field γ called the variogram. We take into account information from all the realizations to infer a single and robust climatological variogram (Lebel et al. 1987). The estimation variance, corresponding to the sampling error, allows assessment of the estimation quality as function of the spatial structure of the rain field and the relative position of the rain gauge network versus the geographical support of interest A . The estimation variance requires the numerical evaluation of two integrals of the variogram function over the domain A (Journel and Huijbregts 1978). Its expression is

$$\begin{aligned} \text{Var}[R_{\text{ref}}(T, A) - R(T, A)] = & -\frac{1}{a^2} \int_A \int_A \gamma(\mathbf{x}, \mathbf{x}') d\mathbf{x} d\mathbf{x}' \\ & + 2 \sum_{j=1}^{N_g} \lambda^j \left[\frac{1}{a} \int_A \gamma(\mathbf{x}, x_j) d\mathbf{x} \right] \\ & - \sum_{i=1}^{N_g} \sum_{j=1}^{N_g} \lambda^i \lambda^j \gamma_{ij}, \end{aligned} \quad (4)$$

where $R(T, A)$ is the true area-averaged rainfall accumulation for the period T and area A , \mathbf{x} is the location vector and x_j denotes the location of the gauge j , a is the area of the domain A , and $\gamma(\mathbf{x}, \mathbf{x}')$ is the variogram function computed on the Euclidean interdistance between the two locations \mathbf{x} and \mathbf{x}' . The first term denotes the block-to-block computation of the variogram function over the domain A , with \mathbf{x} and \mathbf{x}' belonging to A ; the second term corresponds to the computation of the variogram function between each gauge and the domain A ; and the last term is the in-between gauge variogram computation. The estimation variance depends on the variogram characteristics, which are related to the rain field variance. The spatial structures and the variances of rain fields are linked to the integration time period considered (Lebel et al. 1987; Berne et al. 2004; Ali et al. 2005a).

c. The satellite-based rain products

1) THE SATELLITE RAIN ESTIMATES

(i) EPSAT-SG

The Estimation of Precipitation by Satellites-Second Generation (EPSAT-SG) method has been developed at

Laboratoire de Météorologie Dynamique in the framework of the AMMA research program (Bergès et al. 2010). It consists in downscaling the Global Precipitation Climatology Project one-degree daily (GPCP-1DD) product to the Meteosat Second Generation (MSG) spatial and temporal resolutions (3 km and 15 min). It combines a rainfall potential intensity and a rainfall probability derived, because of a feed forward neural network, from the MSG multispectral channels and Tropical Rainfall Measuring Mission (TRMM) Precipitation Radar (PR) information. The product coverage extends from 5°S to 20°N and from 25°W to 25°E , and it is referred to as EPSAT.

(ii) GSMAP

The Global Satellite Mapping of Precipitation (GSMAP) algorithm is inspired by a morphing technique (Joyce et al. 2004) combining passive microwave data from the current fleet of LEO satellite microwave radiometers with cloud motion vectors and brightness temperature from geostationary infrared images. GSMAP covers the globe from 60°N to 60°S at the baseline resolution of $0.1^\circ \times 0.1^\circ$ and 1 h. A description of the methodology can be found in Ushio et al. (2009) and Aonashi and Liu (2000).

(iii) TMPA

The TRMM multiplatform algorithm (TMPA) precipitation dataset is an operational product of the TRMM mission (Huffman et al. 2007). It spans the latitudes from 50°N to 50°S at the resolution of $0.25^\circ \times 0.25^\circ$ and 3 h. It combines precipitation estimates from multiple satellite passive microwave imagers [Special Sensor Microwave Imager (SSM/I), TRMM Microwave Imager (TMI), Advanced Microwave Scanning Radiometer for Earth Observing System (AMSR-E), and Advanced Microwave Sounding Unit-B (AMSU-B)] converted to precipitation estimates using the Goddard profiling algorithm (GPROF; Kummerow et al. 2001), as well as microwave-calibrated infrared precipitation estimate data from the operational fleet of geostationary meteorological satellites. The Global Precipitation Climatology Project monthly rain gauge analysis produced by the Global Precipitation Climatological Center is used for a monthly rescaling (Huffman et al. 1997).

2) THE ERROR MODEL

The evaluation of the satellite products sampling errors when averaged at some scales from instantaneous estimates is a difficult task. Several approaches have been explored, all involving the modeling of the spatial covariance functions of the rain field or its autocorrelation function. Direct estimation using the integrated

estimates of the satellite rain retrievals and the “true” rain fields (Bell et al. 1990; North and Nakamoto 1989) or derivation from the discrepancy between the gauges data and the true rain field (Ali et al. 2005b) are among those. North and Nakamoto (1989) developed a spectral formalism to derive a general expression of the sampling errors, which can be interpreted in the Fourier space–time domain as the covariance rain field filtered by a function depending on the rain field sampling scheme. This expression reduces to the well-known expression of the uncertainty on the estimation of the mean of independent data in cases of simple sampling scheme,

$$\sigma = \frac{S}{\sqrt{N_{\text{ind}}}}, \quad (5)$$

where S is the standard deviation of the samples and N_{ind} is the number of independent data (e.g., Larsen and Marx 2001). Bell et al. (1990) used a stochastic and parametric model of the covariance field with Global Atmospheric Program Atlantic Tropical Experiment (GATE) data to estimate the uncertainties expected at monthly scale and various spatial scales. Bell and Kundu (2003) further used this model to compare different sampling schemes of satellite and rain gauge measurements to optimize network design. The error model developed in Morrissey et al. (1995) is close to a kriging technique and uses a variance reduction factor similar to Eq. (4) but without weights, which collapses to the Eq. (5) if the correlation among the samples is zero. The modeling of sampling errors in the case of combined satellite rainfall estimation products become even more complicated because the sampling scheme depends on which data sources are combined but also on the way the algorithm itself combines the data. Huffman (1997) developed an error function at the monthly scale, following North and Nakamoto (1989), based on the computation of a variance of the observations and the evaluation of a number of independent samples. Recently, ensemble methods have been used to estimate satellite rainfall uncertainty (Bellerby and Sun 2005; Teo and Grimes 2007).

Here, a simple error model is developed with a similar approach: it is assumed that the variance of the true precipitation field could be computed as the variance S^2 of the product data for a given area A and during an integration period T . The number of degrees of freedom is estimated independently of the native resolution of the products and depends on the level of autocorrelation of the product data. Over an area A and during a period T , it is defined as

$$N_{\text{ind}} = \frac{A T}{d^2 \tau}, \quad (6)$$

where d and τ are the e -folding space and time distances, respectively, of a structural function computed using the same variogram function as the one used in section 2b(2) assuming isotropy. The variogram functions of the satellite products is calculated over a $5^\circ \times 5^\circ$ region (9° – 14° N, 0° – 5° E) including both the Niamey and Ouémé sites and instantaneous estimations over the whole season are used. Sensitivity tests have shown very little dependence of the calculations to the selected window. An exponential model is fitted to the average variogram to derive the space and time e -folding distances shown in Fig. 3. The e -folding distance is 37 km for TMPA, 41 km for GSMAP, and 85 km for EPSAT (Figs. 3a,c,e). The temporal variograms are computed for GSMAP and EPSAT only and yield e -folding times of 1 and 1.5 h, respectively (Figs. 3b,d). It is not computed for TMPA because its 3-hourly estimates are considered to be independent.

d. Error computation results

The error models provide an estimation of errors at each time step of space–time-averaged satellite rainfall estimates. The time-averaged relative errors of the three satellite products along with the rain gauge are reported in Table 2 for each of the considered scales. The present error estimates are consistent with the sampling errors reported by Gebremichael and Krajewski (2004, 2005) at daily scale over areas of various sizes and using various sampling frequencies. They estimated the sampling errors of 3-hourly sampled rain fields for daily mean values around 140% for $32 \times 32 \text{ km}^2$ area and 30% for $256 \times 256 \text{ km}^2$ area. For daily average from the TMPA product (3-hourly sampling), the present results give 30% over the site of Niamey ($140 \times 180 \text{ km}^2$), 34% over Ouémé ($110 \times 140 \text{ km}^2$), and 94% over the Dakar site ($30 \times 40 \text{ km}^2$). Figure 4 shows the distribution of the errors. The dispersion of errors of the satellite products is comparable to the one of the rain gauge estimates but is larger for TMPA. The errors are not normally distributed. The relative errors decrease with increasing space–time-averaged rainfall estimate, following a power law similar to that reported in Huffman (1997). Because of its small extension and high density, the subset site of Dakar stands out with the smallest sampling errors for the rain gauges and the largest for the satellite estimates. The ratio of the mean error to the variance of the time series is shown in Table 3. It varies from 0% to 50% depending on the considered scale and product, and it further confirms the need to account for the errors in running the comparison as discussed in section 2a.

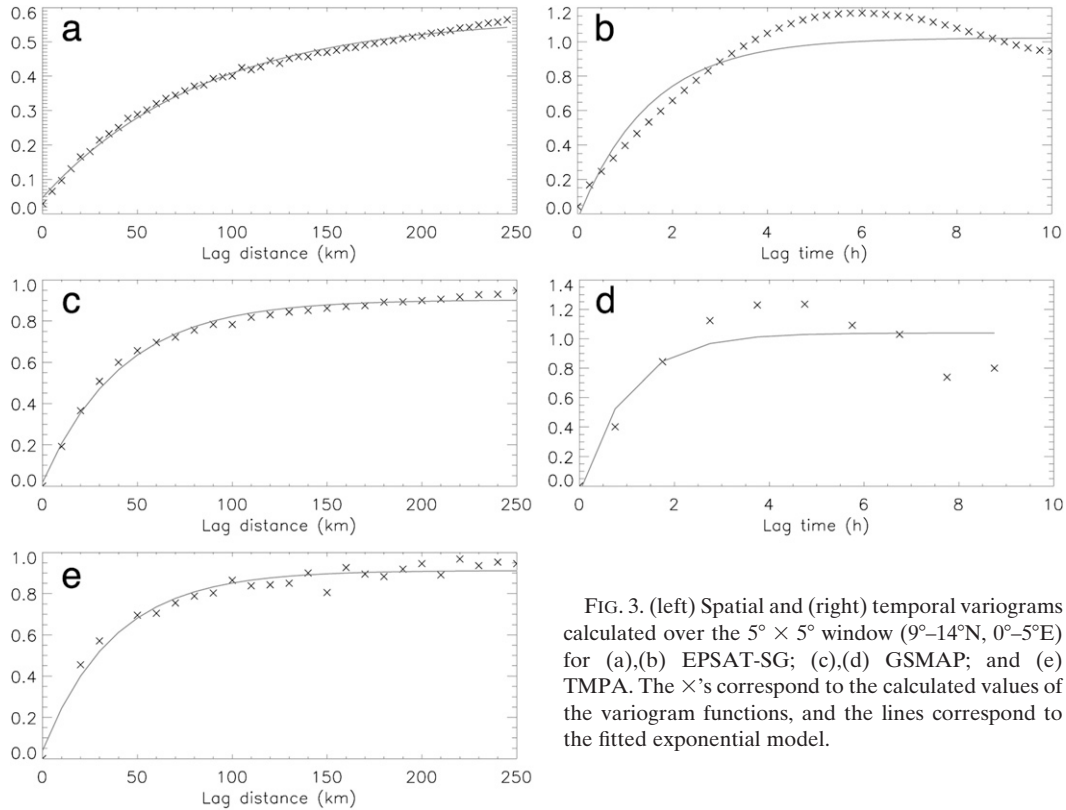


FIG. 3. (left) Spatial and (right) temporal variograms calculated over the $5^{\circ} \times 5^{\circ}$ window (9° – 14° N, 0° – 5° E) for (a),(b) EPSAT-SG; (c),(d) GSMAP; and (e) TMPA. The \times 's correspond to the calculated values of the variogram functions, and the lines correspond to the fitted exponential model.

3. Methodology of comparisons using error estimates

a. Approach

The comparison between the satellite products and the ground rainfall estimates are performed taking into account their respective estimated errors. The rain gauges data are considered as the reference, and the satellite estimates are expected to resemble this reference. Statistics are hence computed to characterize the expected linear relationship between them and the departures from this

one-to-one relationship. First, a linear regression approach has been selected, and the results of this regression are compared to the perfect agreement $y = x$ line. Although linear regression between two samples of data assuming some errors on one of them is readily accessible, the problem is less trivial when assuming errors on both samples. Leng et al. (2007) reviewed the most useful classical techniques to overcome this issue (ordinary least squared, orthogonal regression, etc.) and their respective underlying validity assumptions. These are difficult to meet (e.g., Carroll and Ruppert 1996). As

TABLE 2. Mean percentages of errors for the seasonal diurnal, 10-day, 1-day, and 3-hourly time scales for the gauge and satellite product estimates.

Scale	Site	Gauge	EPSAT	GSMAP	TMPA
Diurnal composite (postonset)	Niamey	4	23	21	31
	Ouémé	3	22	20	31
	Dakar	9	46	74	139
10 days (1–10 Aug 2006)	CILSS	27	17	13	20
10 days (10–21 Jun 2006)	CILSS	86	32	27	32
1 day ($>0.1 \text{ mm h}^{-1}$)	Niamey	21	28	18	30
	Ouémé	17	34	20	34
	Dakar	8	50	61	94
3 hourly ($>0.1 \text{ mm h}^{-1}$)	Niamey	13	54	26	38
	Ouémé	19	88	35	50
	Dakar	15	115	76	69

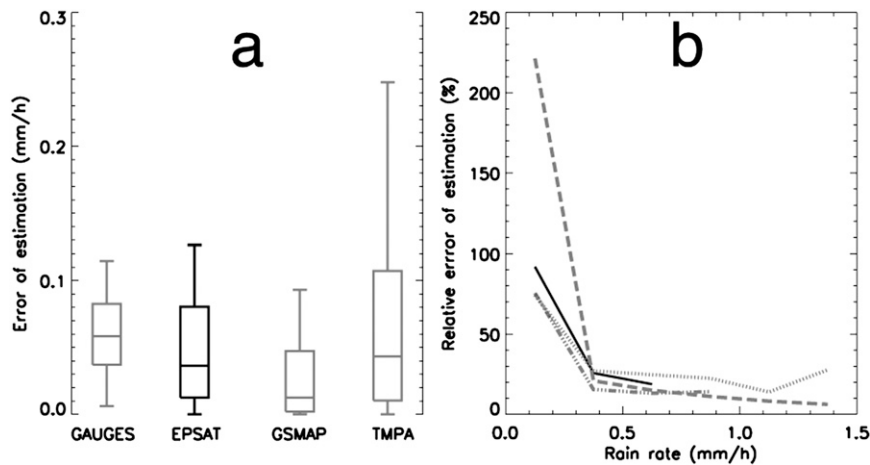


FIG. 4. (a) Box plots of the error of estimation on the gauge and satellite daily estimates over Niamey. Each box shows the 25th and 75th percentiles of the uncertainty distributions. The horizontal line shows the median of the distributions, and the whiskers extend out to largest and smallest values within 1.5 times the interquartile range. (b) Relative errors as a function of rain rate for the gauges (dashed line), EPSAT (solid line), GSMAP (dashed-dotted line), and TMPA (dotted line).

shown in the previous section, here the errors from the satellite estimates are not Gaussian and are not directly comparable to the ground reference ones. The approach of Kelly (2007) has been chosen instead. It requires no assumption on the distribution of errors and is based on a maximum likelihood estimate technique, and a structural linear model (or equation) is used. Noting η as the dependent variable, it is related to ξ following

$$\eta_i = b + a\xi_i + E_i, \quad (7)$$

where E_i is a random variable representing the intrinsic scatter of the regression relationship and a and b are the linear regression coefficients. The mean of E_i is assumed to be zero, and the variance of E_i is assumed to be constant. The measurements data are usually accompanied by error estimates. Noting that x and y are the measurement data and that $E_{x,i}$ and $E_{y,i}$ are the associated errors on x_i and y_i , respectively, their relationship to ξ and η reads as follows:

$$\begin{aligned} x_i &= \xi_i + E_{x,i} \quad \text{and} \\ y_i &= \eta_i + E_{y,i}. \end{aligned} \quad (8)$$

A Bayesian method is used to solve the regression using an elaborated implementation, which is described at length in Kelly (2007). In the present case, $E_{x,i}$ and $E_{y,i}$ are the errors presented in the previous section for the gauges and satellites, respectively.

b. Score indices

Among the various “scoring” indices available to quantify the degree of agreement between the satellite

and rain gauge estimates (Ebert 2007), a subset is selected that relies on the direct—or indirect through the fitting technique—use of the individual errors (for another selection, see Kelly 2007). Hence, the following indices are kept for the analysis:

- the mean coefficient of correlation R and
- the mean slope and mean intercept of the regression line a and b .

The distributions of the coefficients a , b , and R , which are available from Kelly’s technique, were analyzed and the significance of the mean values of the three coefficients were confirmed; they are thus used in the following. From these coefficients, two more indices are computed, the bias and the root-mean-square error (RMSE) of the regression:

TABLE 3. Ratio (%) of the mean error to the variance of the precipitation estimates. For Dakar, the median of the error distributions of the daily estimates is computed rather than the mean error because the latter does not represent the distribution of errors well as a result of the small sample size.

Scale	Site	Gauge	EPSAT	GSMAP	TMPA
10 day (1–10 Aug 2006)	CILSS	34	11	5	12
10 day (10–21 Jun 2006)	CILSS	26	10	5	17
1 day	Niamey	4	18	4	13
	Ouémé	3	19	4	16
	Dakar	0.2	45	14	14
3 hourly	Niamey	0.6	25	4	12
	Ouémé	1	42	7	12
	Dakar	0.3	72	32	84

- the bias of the regression is $\text{BIAS-reg} = b + (a - 1) \text{Rain}_G$, where Rain_G is the average value of the gauge estimates, and
- the root-mean-square of the regression is $\text{RMS-reg} = (1 - R^2)^{0.5} S_y^{0.5}$, where S_y is the variance of the satellite product.

Because the bias and the root-mean-square of the regression are functions of the coefficients a , b , and R , they indirectly account for the individual errors.

Similarly, the well-used probability of detection of rain (POD) and false-alarm rate (FAR) indices have been adapted to this error context for the analysis of the daily scale. Finally, a new index is computed. It consists in the frequency of error bars overlap (FEBO). The error bars are interpreted as a confidence interval, and FEBO represents the frequency of cases for which the satellite and the ground estimate error bars overlap. FEBO equals 1 if the two series are close enough given their errors and 0 if none of the values are close. FEBO is computed on the raw series as well as on the unbiased series. Both the regression and the FEBO computations are run systematically for the time-accumulated comparison over the whole Sahel as well as for the daily average comparisons over the three dense rain gauge network sites. All the regressions are computed only for the conditional rainfall estimates.

4. Results

The results in this section described the ability of the satellite products to mimic the rainfall variability derived from the gauges. The variability is investigated at various scales of accumulation. First, the seasonal cycle is analyzed using 10-day-averaged products, then the synoptic-scale variability is analyzed using daily means, and finally the diurnal cycle of rainfall is analyzed at both the seasonal scale using a composite and at the diurnal scale using 3-hourly accumulations.

a. Monsoon preonset and postonset and seasonal scales

In 2006, the monsoon onset occurred between 4 and 10 July (Janicot et al. 2008). Therefore two 10-day periods were arbitrarily selected as representative of the conditions of the preonset (11–20 June) and postonset (1–10 August) to analyze the 10-day accumulation seasonal variability. The results of the comparison are presented in Table 4. For the second period, high correlation coefficients are found for the three satellite products with similar values for EPSAT and TMPA ($R \sim 0.95$). By contrast, correlations calculated without errors (not

TABLE 4. Statistics of the regressions between the three satellite products and the gauge estimates (i) for the 10-day period (11–20 Jun 2006) and (ii) for the 10-day period (1–10 Aug 2006). Sample size = 137.

(i) 11–20 Jun 2006	EPSAT	GSMAP	TMPA
Correlation	0.97	0.81	0.96
Slope	0.95	0.81	0.83
Intercept (mm h^{-1})	-0.02	-0.01	-0.00
BIAS-reg (mm h^{-1})	-0.02	-0.02	-0.01
RMS-reg (mm h^{-1})	0.01	0.03	0.02
FEBO	0.77	0.58	0.75
FEBO unbiased	0.77	0.65	0.75
(ii) 1–10 Aug 2006	EPSAT	GSMAP	TMPA
Correlation	0.98	0.82	0.93
Slope	1.15	0.80	1.29
Intercept (mm h^{-1})	-0.08	-0.06	-0.11
BIAS-reg (mm h^{-1})	-0.04	-0.12	-0.03
RMS-reg (mm h^{-1})	0.02	0.05	0.05
FEBO	0.82	0.35	0.69
FEBO unbiased	0.84	0.64	0.69

shown) were significantly lower but similar for GSMAP and TMPA. The biases are all negatives, with a bias of -0.12 mm h^{-1} for GSMAP and equivalent lower values for EPSAT (-0.04 mm h^{-1}) and TMPA (-0.03 mm h^{-1}). Figure 5 shows the scatter diagram of the satellite versus gauge products for the second period. The error bars and the regression line are also plotted. A no-error regression line is also reported (dashed line). It shows that EPSAT and TMPA suffer from overestimation of the large precipitation intensities. If the error bars had not been taken into account into the regression process, the result would have been the opposite. The RMS-reg is 0.02 mm h^{-1} for EPSAT but 0.05 mm h^{-1} for GSMAP and TMPA, meaning a higher precision in the fitted linear model for EPSAT. The FEBO index shows an agreement greater than 80% in both biased and unbiased cases for EPSAT. If GSMAP has the lowest linear performance scores, and similar unbiased agreements larger than 60% are found for TMPA and GSMAP. Statistics for the first period (preonset) yield similar conclusions but with smaller biases and RMS-reg values. At this 10-day scale, the satellite products capture the regional and seasonal variability of the gauges.

b. Synoptic scales

1) DAILY TIME SERIES

Both the satellite and gauge daily time series are characterized by a succession of days with and without rain. The POD and FAR allow the agreement between the two time series to be quantified, but the two indices have to be

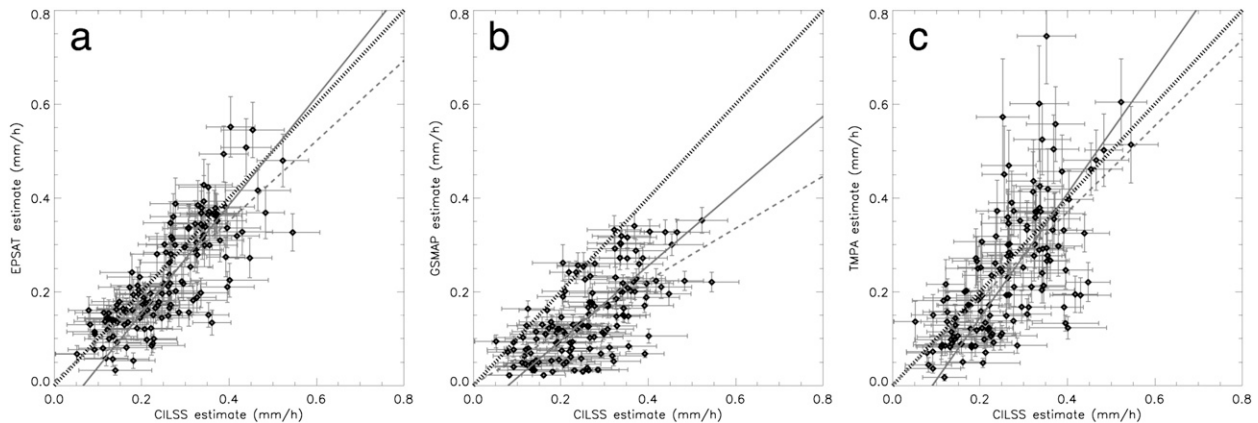


FIG. 5. Scattergrams of the 10-day rainfall (a) EPSAT, (b) GSMAP, and (c) TMPA estimates vs CILSS rain gauge estimates (mm h^{-1}) for the 1–10 Aug 2006 period. One-sigma error bars are over plotted. The thin solid line is the regression line taking the error bars into account, and the dashed line is without the errors. The thick solid line is the 1:1 line.

adapted to account for the errors. In fact, as seen in section 2d, the error can be larger than the rain estimate itself for the small values. In such a case, the rainy day, because of the error, could also be considered as a non rainy day. Hence, POD and FAR must be computed using a variety of time series accounting for various numbers of non rainy days. Thus, a probability distribution function of POD and FAR values is considered; in the following results, we give only the respective worst values: that is, the smallest POD and the largest FAR values.

The regression computation accounting for errors, described in section 3a, is applied to the time series limited to the rainy days in both series (satellite and gauges). The scatterplots are shown in Fig. 6 for the three products and the three sites. The results of the statistical parameters described in section 3b along with FAR, POD, and FEBO indices are given in Table 5.

Figures 6a–f, over Niamey and Ouémé, indicate a general underestimation of the large precipitation intensities. In Figs. 6g–i, it is noticeable that, for the site of Dakar, the errors are small for the rain gauges because of the high density of the network, whereas the satellite products errors are large because of the small size of the Dakar site area. These large errors have an important impact on the characteristics of the regression accounting for the errors, which can be seen by the strong difference between the regression line (full line) with errors and the regression line (dashed line) without errors.

Considering the correlation coefficients, they are of the same order for EPSAT and TMPA and almost as high as for the 10-day accumulations. The correlation coefficients are lower for GSMAP, at least for Niamey and Ouémé. Similarly, considering the biases (BIAS-reg), EPSAT and TMPA provide the same order of negative bias (ranging from -0.04 to -0.08 mm h^{-1}), much smaller than the

biases for GSMAP (-0.14 and -0.21 mm h^{-1}). The RMS-reg values obtained for EPSAT range between 0.09 and 0.12 mm h^{-1} , the ones for GSMAP range between 0.10 and 0.18 mm h^{-1} , and the ones for TMPA range between 0.21 and 0.25 mm h^{-1} . EPSAT present the worst values of FAR (ranging from 34% to 56%) over the three sites but also the largest POD values, over 92% for Niamey and Ouémé. The POD values are slightly lower for the two other products. Finally, the FEBO values show lower skills than for the 10-day scale, ranging from 24% to 64% over Niamey and Ouémé. The FEBO unbiased values are always lower than their corresponding FEBO but have a similar range.

To summarize, the statistics are consistent over Niamey and Ouémé but lead to different conclusions over the site of Dakar. In addition, its smaller extension, the period considered for Dakar, is also shorter, which results in smaller sample sizes giving less strength to the statistics. In general, these results show that EPSAT and TMPA have similar skills at the daily scale, whereas regression characteristics of GSMAP are lower over Niamey and Ouémé.

2) 3–5-DAY FILTERED TIME SERIES

The ability of the satellite products to reproduce the well-recognized mode of synoptic variability of rainfall associated with the passing of AEW compared to the gauges is quantified by using simple spectral filtering of the 3–5-day band for each estimate. Figure 7 exemplifies the results for Ouémé and shows that indeed very good agreement is found at this scale. Both EPSAT and GSMAP tend to underestimate the high rain rates, whereas TMPA tends to overestimate them. The overall good agreement is confirmed by the statistics reported in Table 5 where high correlation, low bias, and RMS are

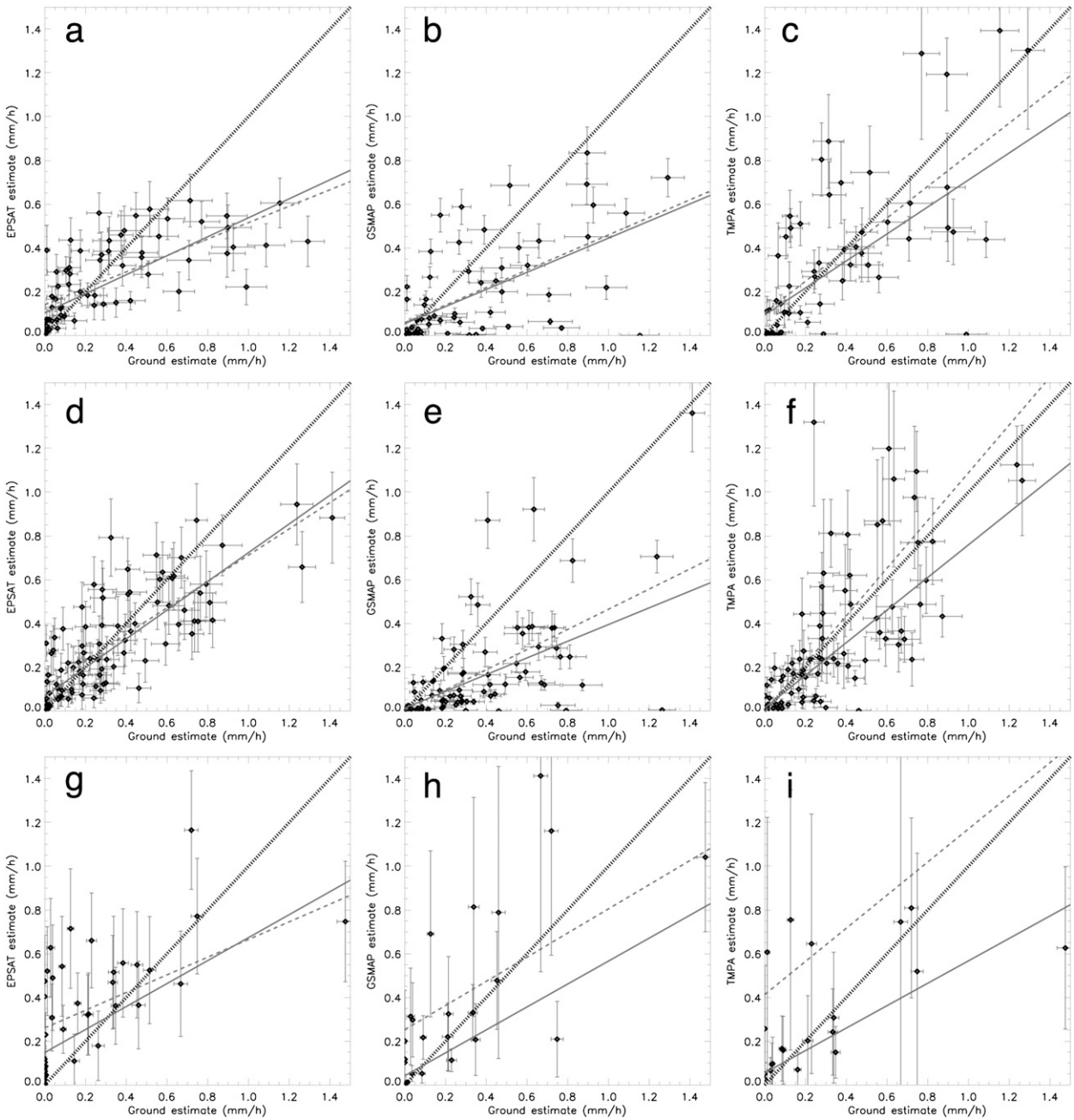


FIG. 6. Scattergrams of the daily rainfall (mm h^{-1}) of (left) EPSAT, (middle) GSMAP, and (right) TMPA estimates over the sites of (a)–(c) Niamey, (d)–(f) Ouémé, and (g)–(i) Dakar. One-sigma error bars are overplotted. The thin solid line is the regression line taking the error bars into account, and the dashed line is without the errors. The thick solid line is the 1:1 line.

reported. Over the Ouémé and Niamey sites, EPSAT and TMPA outperform GSMAP, which reveals a slightly worse overall fit to the gauges. At Dakar, the scores are still high, although less than for the previous sites, as expected from the smaller network under consideration (see section 2d). Again, GSMAP exhibits less skill than the other products. Generally, the satellite

estimates reproduce well the rainfall variability resulting from AEW, better than the unfiltered synoptic data.

c. Diurnal scale

An index is computed to quantify the influence of diurnal cycle of the insolation on rainfall. A simple Fourier analysis is performed on the 3-hourly time

TABLE 5. Statistics of the regressions between the three satellite products and the gauge daily rain estimates and between the three satellite products and the gauge filtered (3–5 days) daily rain estimates over Niamey, Ouémé, and Dakar.

	Daily estimates			Filtered (3–5 days) daily estimates		
	EPSAT	GSMAP	TMPA	EPSAT	GSMAP	TMPA
Niamey						
Correlation	0.83	0.61	0.72	0.91	0.81	0.86
Slope	0.43	0.39	0.61	0.50	0.51	0.82
Intercept (mm h ⁻¹)	0.10	0.05	0.09	0.07	0.02	0.03
BIAS-reg (mm h ⁻¹)	-0.07	-0.14	-0.04	-0.04	-0.09	-0.02
RMS-reg (mm h ⁻¹)	0.10	0.18	0.25	0.03	0.06	0.07
FAR	0.56	0.40	0.40	—	—	—
POD	0.92	0.83	0.79	—	—	—
FEBO	0.55	0.43	0.53	0.75	0.48	0.77
FEBO unbiased	0.40	0.24	0.53	0.78	0.64	0.77
Sample size	67	63	57	67	63	57
Ouémé						
Correlation	0.92	0.64	0.90	0.92	0.71	0.95
Slope	0.66	0.38	0.75	0.68	0.44	1.24
Intercept (mm h ⁻¹)	0.07	0.01	0.01	0.06	0.01	-0.03
BIAS-reg (mm h ⁻¹)	-0.05	-0.21	-0.08	-0.07	-0.12	-0.02
RMS-reg (mm h ⁻¹)	0.09	0.18	0.21	0.05	0.08	0.14
FAR	0.34	0.26	0.29	—	—	—
POD	0.93	0.81	0.90	—	—	—
FEBO	0.64	0.25	0.56	0.80	0.25	0.78
FEBO unbiased	0.56	0.30	0.48	0.79	0.63	0.80
Sample size	89	81	81	89	81	81
Dakar						
Correlation	0.89	0.97	0.96	0.85	0.65	0.71
Slope	0.53	0.52	0.51	0.68	0.63	0.95
Intercept	0.15	0.04	0.06	0.13	0.13	0.11
BIAS-reg (mm h ⁻¹)	0.03	-0.12	-0.12	0.07	0.05	0.10
RMS-reg (mm h ⁻¹)	0.12	0.10	0.23	0.07	0.11	0.26
FAR	0.56	0.32	0.15	—	—	—
POD	0.76	0.59	0.32	—	—	—
FEBO	0.55	0.56	0.88	0.70	0.815	0.84
FEBO unbiased	0.58	0.56	0.48	0.80	0.85	0.68
Sample size	40	27	25	40	27	25

series, and all the scales less than or equal to one day are low-pass filtered. The filtered time series is then correlated with the raw series using the same method as earlier. The original errors at 3 h are used for both the original and the filtered series. The coefficient of determination R^2 provides the fraction of the common variance between the two series; subtracted from 1, it gives the fraction of variance associated with the diurnal scale. Results are summarized in Table 6. As expected, the gauges confirm the important role of the diurnal scale in the total variance of the rainfall field with value around 64% for Niamey after the onset. The satellite products also show such strong contributions of the diurnal scale. At Niamey, the satellite products all show a stronger contribution of the diurnal cycle after the onset (Mathon et al. 2002). At Ouémé, ground measurements reveal a stronger contribution before the onset than after, and the satellite estimates do not reveal a consistent behavior. This is consistent with the findings of Depraetere et al. (2009)

based on systems tracking at ground using gauges and radar. At Dakar, the gauge network indicates a 43% fraction, which TMPA reproduces well and is overestimated in both EPSAT and GSMAP.

The composite or mean diurnal cycle is further computed and presented in Fig. 8. Before the onset, the mean cycle is very flat over both Sahelian regions; when the monsoon has come, Niamey exhibits a marked late night–early morning maximum and Ouémé shows a maximum, although smoother, occurring between 15 and 18 h. Over Dakar, the rain peaks between 15 and 21 h are presumably associated with local convection rather than traveling systems (e.g., Jenkins et al. 2010, unpublished manuscript). The satellite products rather exhibit a smooth maximum during the night, but TMPA also reproduces the late afternoon maximum. Note that, because of the small size of the analyzed region, the satellite estimates here are prone to large errors that make the comparison less direct. These well-documented features of the WAM diurnal

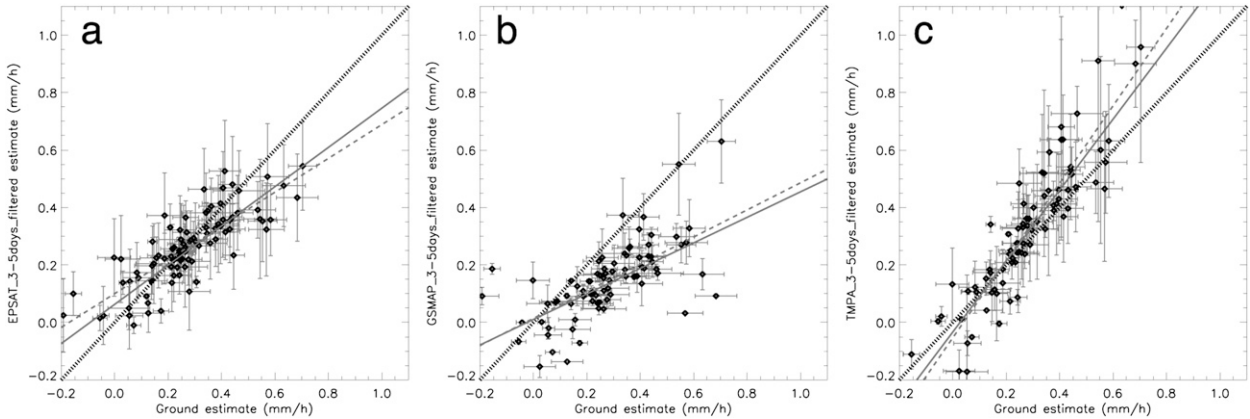


FIG. 7. Scattergrams of the 3–5-day filtered daily rainfall (mm h^{-1}) of (a) EPSAT, (b) GSMAP, and (c) TMPA estimates vs the 3–5-day filtered daily rainfall gauge estimates over the Ouémé site. One-sigma error bars are over plotted. The thin solid line is the regression line taking the error bars into account, and the dashed line is without the errors. The thick solid line is the 1:1 line.

cycle are thought to be associated with a shift in the nature of the convective events with well-organized squall lines, initiated eastward and earlier in the day, contributing to this night time maximum for Niamey after the onset (Fink and Reiner 2003). Generally, the satellite products capture well this seasonal variability in the composite diurnal cycle (Fig. 8). For Niamey, the three products roughly behave similarly as indicated by the computation of the FEBO reported in Table 7. For Ouémé and Dakar, only TMPA captures the gauges features. Overall, TMPA has the higher FEBO statistics followed by EPSAT and GSMAP, which resemble each other.

The fraction of common variance between the original time series and the time series from which the mean cycle is repeatedly subtracted highlight the significance of the composite diurnal cycle (Nesbitt and Zipser 2003). The stronger contribution of the composite cycle is found in the gauges for Dakar with a value of 34% (Table 8). The satellite estimates reproduce this, but for the EPSAT product the composite cycle hardly contributes to the variance. For Niamey, gauges indicate a 13% contribution of the mean cycle that is not seen in the EPSAT results. GSMAP and TMPA overestimate ($\sim 37\%$) their composite cycle influence. For Ouémé, the mean cycle only weakly contributes to the variance, a fact that satellite products agree upon only after the onset. Over the preceding period, both GSMAP and TMPA show a significant contribution of their respective composite cycles, which are very flat (Fig. 8c). The detailed analysis nevertheless reveals that the TMPA products best behave with respect to the gauges than other satellite products. Such good behavior of this product was previously noted over the Gulf of Mexico and was attributed to the final adjustment step that relies on the monthly gauges analysis (Sapiano and Arkin 2009).

5. Summary and discussion

Ground data and satellite products of surface rainfall have been compared using a novel approach that accounts for the errors in the areal mean rainfall estimates during the AMMA 2006 campaign. The analysis focused on three well-instrumented sites covering a wide range of rain regimes. Simple sampling error models based on the spatial and temporal correlations of the rain field have been used both for the gauges (block kriging) and for the satellite estimates (variograms). This study completes previous efforts with climatic (e.g., Nesbitt et al. 2004) and hydrologic (Hossain and Huffman 2008) perspectives by focusing on the meteorological scales relevant to the WAM. The findings of this study are as follows:

- at a $1^\circ \times 1^\circ$ scale, the block-kriging errors varies from 4% to 86% depending on the accumulation time and less than 15% over the denser network at Dakar;

TABLE 6. Percentage of variance explained by the subdaily variability of the gauge rain rate and of the three rainfall satellite products during the postonset and preonset periods for the sites of Niamey, Ouémé, and Dakar. The variance explained is calculated as $1 - R^2$, where R is the correlation between the 1-day low-pass filtered 3-hourly time series and the 3-hourly time series. Low values ($<0.1 \text{ mm h}^{-1}$) are filtered out, yielding to a varying population to perform the computations.

Site	Period	Gauge	EPSAT	GSMAP	TMPA
Niamey	Postonset	64	32	48	54
	Preonset	26*	31	27	44
Ouémé	Postonset	36	32	16	67
	Preonset	61	30	56*	25
Dakar	1 Aug–30 Sep	43	37	80*	43

* Not significant at the 99.9% level.

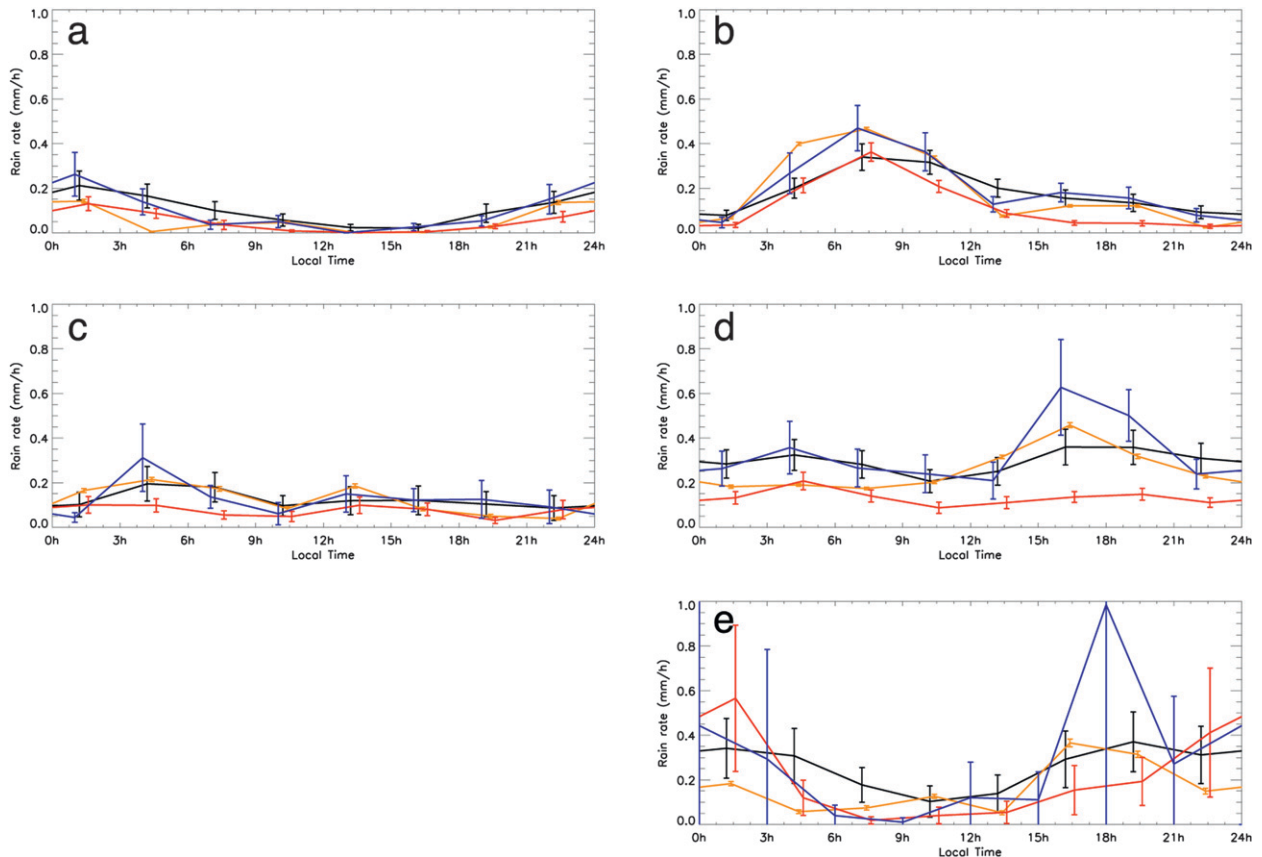


FIG. 8. Composite diurnal cycles of rain rates obtained from Gauges (orange line), EPSAT (black line), GSMAP (red line), and TMPA (blue line) for the (left) preonset and (right) postonset periods for (a),(b) Niamey; (c),(d) Ouémé, and (e) Dakar. Two-sigma error bars are plotted over the lines.

- the satellite errors are of the same order as the gauges errors, except for the smallest network, over which the satellite errors are greater;
- at a 10-day scale, all the tested products show high skill in reproducing the ground network results, including the preonset–postonset variability;
- at a daily scale, satellite products skill range from high to moderate;
- at the AEW scale, all the tested products show high skill in reproducing the ground network variability; and
- the mean diurnal cycle and its variability in space and during the season are relatively well captured by some products, and others revealed difficulty to account for such scale.

Over the range of scales and rain regimes and types discussed here, the combined IR–MW satellite products are describing the rain variability similar to that of the ground measurements, with some being better than others at different scales. These products can then be used to investigate the physical functioning of the monsoon. For instance, Peyrillé et al. (2007) and Peyrillé and Lafore

(2007) established an idealized conceptual model of the WAM to analyze the seasonal and diurnal cycle of the monsoonal rainfall that can be confronted to these satellite products. Using the National Centers for Environmental Prediction (NCEP) operational analysis, Bielli and Roca (2009) reported during the summer 2006 a lead–lag relationship between surface evaporation and rainfall in the WAM characterized by regional and temporal scale dependence (AEW). The use of the satellite products in such a water budget analysis would greatly enhance the findings of this model-based analysis. Yang and Smith (2006) provide an extensive, perhaps exhaustive, review on the physical processes associated to the diurnal variability of rainfall over the whole tropics. Elucidating the relative role of the various diurnal mechanisms for the whole West African monsoon region can now be attempted using the strength (coverage and sampling) of the validated new generation of combined satellite level 2 products.

The present methodology could easily be applied again if a better estimation of the error budget becomes available. The elaboration of our simple error sampling

TABLE 7. FEBO and FEBO unbiased indices calculated with the mean diurnal cycles of EPSAT, GSMAP, and TMPA with 2-sigma errors.

Site	Period		EPSAT	GSMAP	TMPA	
Niamey	Postonset	FEBO	0.50	0.25	0.50	
		FEBO unbiased	0.38	0.38	0.38	
	Preonset	FEBO	0.50	0.62	0.62	
		FEBO unbiased	0.50	0.50	0.50	
	Ouémé	Postonset	FEBO	0.38	0.12	0.50
			FEBO unbiased	0.50	0.25	0.88
Preonset		FEBO	1.00	0.38	0.88	
		FEBO unbiased	0.88	0.38	0.88	
Dakar	1 Aug–30 Sep	FEBO	0.50	0.38	0.75	
		FEBO unbiased	0.62	0.38	0.62	

model toward a more complete error model (including the algorithm error term) is one venue for future research. An extension of the present effort to a larger number of years and satellite products making use of the ground data of the EOP of the AMMA program could strengthen the present results, especially for diurnal cycle prone to large interannual fluctuations (Mohr 2004). Finally, the documentation of the individual convective system scale ($\Delta t < 1$ h; $\Delta x \sim 10$ km) at which rain radar, gauges, and satellites provide different perspectives, which are difficult to compare (e.g., Roca et al. 2010), should be undertaken. The present error-based approach might be one way to improve on the situation, but such downscaling would require the challenging estimation of an error budget at finer scale.

Acknowledgments. We are very much indebted to the crew that operated the AMMA CATCH ground networks during the summer, especially Guillaume Quantin and Leandro Suarez who processed the data for the Niamey, Niger, and the Ouémé, Benin, areas. The data from Dakar were made available to us by A. T. Gaye from the Laboratoire de Physique de l'Atmosphère et de l'Océan Siméon Fongang. We thank the AGRHYMET centre and the affiliated African Meteorological Services for providing us with the gridded fields of 10-day precipitation used as validation dataset for this study, particularly Dr. A. Ali. Helpful discussion with the LMD AMMA group and Dr. N. Viltard is acknowledged. We are grateful to Dr. B. C. Kelly for making his IDL fitting routine available. Based on a French initiative AMMA was built by an international scientific group and is currently funded by a large number of agencies, especially from France, United Kingdom, United States, and Africa.

TABLE 8. Percentage of variance explained by the mean conditional diurnal cycle of the Gauge rain rate and of the three rainfall satellite products during the postonset and preonset periods for the sites of Niamey, Ouémé, and Dakar. The variance explained is calculated as $1 - R^2$, where R is the correlation between the 3-hourly time series anomalies to the mean conditional diurnal cycle and the 3-hourly time series.

Site	Period	Gauge	EPSAT	GSMAP	TMPA
Niamey	Postonset	13	0.8	38	36
	Preonset	34*	7	23	56
Ouémé	Postonset	3	1	3	4.7
	Preonset	6	2	46*	31
Dakar	1 Aug–30 Sep	34	0.9	60	27

* Not significant at the 99.9% level.

It has been the beneficiary of a major financial contribution from the European Community's Sixth Framework Research Programme.

REFERENCES

- Ali, A., and T. Lebel, 2008: The Sahelian standardized rainfall index revisited. *Int. J. Climatol.*, **29**, 1705–1714, doi:10.1002/joc.1832.
- , —, and A. Amani, 2005a: Rainfall estimation in the Sahel. Part I: Error function. *J. Appl. Meteor.*, **44**, 1691–1706.
- , A. Amani, A. Diedhiou, and T. Lebel, 2005b: Rainfall estimation in the Sahel. Part II: Evaluation of rain gauge networks in the CILSS countries and objective intercomparison of rainfall products. *J. Appl. Meteor.*, **44**, 1707–1722.
- Aonashi, K., and G. Liu, 2000: Passive microwave precipitation retrievals using TMI during the Baiu period of 1998. Part I: Algorithm description and validation. *J. Appl. Meteor.*, **39**, 2024–2037.
- Bell, T. L., and P. K. Kundu, 2003: Comparing satellite rainfall estimates with rain gauge data: Optimal strategies suggested by a spectral model. *J. Geophys. Res.*, **108**, 4121, doi:10.1029/2002JD002641.
- , A. Abdullah, R. L. Martin, and G. R. North, 1990: Sampling errors for satellite-derived tropical rainfall: Monte Carlo study using a space-time stochastic model. *J. Geophys. Res.*, **95**, 2195–2205.
- Bellerby, T. J., and J. Sun, 2005: Probabilistic and ensemble representations of the uncertainty of the IR/microwave satellite precipitation product. *J. Appl. Meteor.*, **6**, 1032–1044.
- Bergès, J. C., F. Chopin, I. Jobard, and R. Roca, 2010: EPSAT-SG: A satellite method for precipitation estimation; its concept and implementation for AMMA experiment. *Ann. Geophys.*, **28**, 289–308.
- Berne, A., G. Delrieu, J. D. Creutin, and C. Obled, 2004: Temporal and spatial resolution of rainfall measurements required for urban hydrology. *J. Hydrol.*, **299**, 166–179.
- Bielli, S., and R. Roca, 2009: Scale decomposition of atmospheric water budget over West Africa during the monsoon 2006 from NCEP/GFS analyses. *Climate Dyn.*, doi:10.1007/s00382-009-0597-5.
- Carroll, R. J., and D. Ruppert, 1996: The use and misuse of orthogonal regression estimation in linear errors-in-variables models. *Amer. Stat.*, **50**, 1–6.

- Ciach, G. J., 2003: Local random errors in tipping-bucket rain gauge measurements. *J. Atmos. Oceanic Technol.*, **20**, 752–759.
- , and W. F. Krajewski, 1999: On the estimation of radar rainfall error variance. *Adv. Water Res.*, **22**, 585–595.
- Conway, D., A. Persechino, S. Ardoin-Bardin, H. Hamandawana, C. Dieulin, and G. Mahé, 2009: Rainfall and water resources variability in sub-Saharan Africa during the twentieth century. *J. Hydrometeorol.*, **10**, 41–59.
- Depaertere, C., M. Gosset, S. Ploix, and H. Laurent, 2009: The organization and kinematics of tropical rainfall systems ground tracked at mesoscale with gages: First results from the campaigns 1999–2006 on the Upper Ouémé Valley (Benin). *J. Hydrol.*, **375**, 143–160, doi:10.1016/j.jhydrol.2009.01.011.
- Desbois, M., T. Kayiranga, B. Gnamien, S. Guessous, and L. Picon, 1988: Characterization of some elements of the Sahelian climate and their interannual variations for July 1983, 1984 and 1985 from the analysis of METEOSAT ISCCP data. *J. Climate*, **1**, 867–904.
- Ebert, E. E., 2007: Methods for verifying satellite precipitation estimates. *Measuring Precipitation from Space: EURAINSAT and the Future*, V. Levizzani, P. Bauer, and F. J. Turk, Eds., Springer, 345–356.
- , and M. J. Manton, 1998: Performance of satellite rainfall estimation algorithms during TOGA COARE. *J. Atmos. Sci.*, **55**, 1537–1557.
- , —, P. A. Arkin, R. J. Allam, G. E. Holpin, and A. Gruber, 1996: Results from the GPCP algorithm intercomparison projects. *Bull. Amer. Meteor. Soc.*, **77**, 2875–2887.
- , J. E. Janowiak, and C. Kidd, 2007: Comparison of near-real-time precipitation estimates from satellite observations and numerical models. *Bull. Amer. Meteor. Soc.*, **88**, 47–64.
- Fink, A. H., and A. Reiner, 2003: Spatiotemporal variability of the relation between African easterly waves and West African squall lines in 1998 and 1999. *J. Geophys. Res.*, **108**, 4332, doi:10.1029/2002JD002816.
- Gebremichael, M., and W. F. Krajewski, 2004: Characterization of the temporal sampling error in space-time-averaged rainfall estimates from satellites. *J. Geophys. Res.*, **109**, D11110, doi:10.1029/2004JD004509.
- , and —, 2005: Modeling distribution of temporal sampling errors in area-time-averaged rainfall estimates. *Atmos. Res.*, **73**, 243–259.
- Giannini, A., M. Biasutti, I. M. Held, and A. H. Sobel, 2008a: A global perspective on African climate. *Climatic Change*, **90**, 359–383, doi:10.1007/s10584-008-9396-y.
- , —, and M. M. Verstraete, 2008b: A climate model-based review of drought in the Sahel: Desertification, the re-greening and climate change. *Global Planet. Change*, **64**, 119–128, doi:10.1016/j.gloplacha.2008.05.004.
- Grimes, D. I. F., E. Pardo, and R. Bonifacio, 1999: Optimal areal rainfall estimation using rain gauges and satellite data. *J. Hydrol.*, **222**, 93–108.
- Gu, G., and R. F. Adler, 2004: Seasonal evolution and variability associated with the West African monsoon system. *J. Climate*, **17**, 3364–3377.
- , —, G. J. Huffman, and S. Curtis, 2003: Summer synoptic-scale waves over West Africa observed by TRMM. *Geophys. Res. Lett.*, **30**, 1729, doi:10.1029/2003GL017402.
- Habib, E., W. F. Krajewski, and A. Kruger, 2001: Sampling errors of tipping-bucket rain gauge measurements. *J. Hydrol. Eng.*, **6**, 159–166.
- Hastenrath, S., 1991: *Climate Dynamics of the Tropics*. Springer, 488 pp.
- Herman, A., V. B. Kumar, P. A. Arkin, and J. V. Kousky, 1997: Objectively determined 10-day African rainfall estimates created for famine early warning systems. *Int. J. Remote Sens.*, **18**, 2147–2159.
- Hossain, F., and G. J. Huffman, 2008: Investigating error metrics for satellite rainfall data at hydrologically relevant scales. *J. Hydrometeorol.*, **9**, 563–575.
- Hsu, K., X. Gao, S. Sorooshian, and H. V. Gupta, 1997: Precipitation estimation from remotely sensed information using artificial neural networks. *J. Appl. Meteor.*, **36**, 1176–1190.
- Huffman, G. J., 1997: Estimates of root-mean-square random error for finite samples of estimated precipitation. *J. Appl. Meteor.*, **36**, 1191–1201.
- , and Coauthors, 1997: The Global Precipitation Climatology Project (GPCP) combined precipitation dataset. *Bull. Amer. Meteor. Soc.*, **78**, 5–20.
- , R. F. Adler, M. M. Morrissey, D. T. Bolvin, S. Curtis, R. Joyce, B. McGavock, and J. Susskind, 2001: Global precipitation at one-degree daily resolution from multisatellite observations. *J. Hydrol.*, **2**, 36–50.
- , and Coauthors, 2007: The TRMM Multisatellite Precipitation Analysis (TMPA): Quasi-global, multiyear, combined-sensor precipitation estimates at fine scales. *J. Hydrometeorol.*, **8**, 38–55.
- Janicot, S., and Coauthors, 2008: Large-scale overview of the summer monsoon over West Africa during the AMMA field experiment in 2006. *Ann. Geophys.*, **26**, 2569–2595.
- Jenkins, G. S., and A. T. Gaye, 2010: Increasing research opportunities in the atmospheric sciences for underrepresented groups through international field experiences in Senegal. *Bull. Amer. Meteor. Soc.*, in press.
- Jobard, I., and M. Desbois, 1994: Satellite estimation of the tropical precipitation using the Meteosat and SSM/I data. *Atmos. Res.*, **34**, 285–298.
- , F. Chopin, J. C. Bergès, and R. Roca, 2010: An intercomparison of 10-day precipitation satellite products during West African monsoon. *Int. J. Remote Sens.*, in press.
- Journel, A., and C. Huijbregts, 1978: *Mining Geostatistics*. Academic Press, 600 pp.
- Joyce, R., J. E. Janowiak, P. A. Arkin, and P. Xie, 2004: CMORPH: A method that produces global precipitation estimates from passive microwave and infrared data at high spatial and temporal resolution. *J. Hydrometeorol.*, **5**, 487–503.
- Kelly, B. C., 2007: Some aspects of measurement error in linear regression of astronomical data. *Astrophys. J.*, **665**, 1489–1506.
- Kiladis, G. N., C. D. Thorncroft, and N. M. J. Hall, 2006: Three-dimensional structure and dynamics of African easterly waves. Part I: Observations. *J. Atmos. Sci.*, **63**, 2212–2230.
- Kummerow, C., and Coauthors, 2001: The evolution of the Goddard profiling algorithm (GPROF) for rainfall estimation from passive microwave sensors. *J. Appl. Meteor.*, **40**, 1801–1820.
- Lamptey, B. L., 2008: Comparison of gridded multisatellite rainfall estimates with gridded gauge rainfall over West Africa. *J. Appl. Meteor. Climatol.*, **47**, 185–205.
- Larsen, R. J., and M. L. Marx, 2001: *An Introduction to Mathematical Statistics and Its Applications*. 3rd ed. Prentice Hall, 790 pp.
- Laurent, H., I. Jobard, and A. Toma, 1998: Validation of satellite and ground-based estimates of precipitation over the Sahel. *Atmos. Res.*, **47–48**, 651–670.

- Le Barbé, L., T. Lebel, and D. Tapsoba, 2002: Rainfall variability in West Africa during the years 1950–90. *J. Climate*, **15**, 187–202.
- Lebel, T., and A. Amani, 1999: Rainfall estimation in the Sahel: What is the ground truth? *J. Appl. Meteor.*, **38**, 555–568.
- , G. Bastin, C. Obled, and J. D. Creutin, 1987: On the accuracy of areal rainfall estimation: A case study. *Water Resour. Res.*, **23**, 2123–2134.
- , and Coauthors, 2009: AMMA-CATCH studies in the Sahelian region of West-Africa: An overview. *J. Hydrol.*, **375**, 3–13, doi:10.1016/j.jhydrol.2009.03.020.
- , and Coauthors, 2010: The AMMA field campaigns: Multi-scale and multidisciplinary observations in the West African region. *Quart. J. Roy. Meteor. Soc.*, **136** (Supp. S1), 8–33.
- Leng, L., T. Zhang, L. Kleinman, and W. Zhu, 2007: Ordinary least square regression, orthogonal regression, geometric mean regression and their application in aerosol science. *J. Phys.*, **78**, 012084, doi:10.1088/1742-6596/78/1/012084.
- Levizzani, V., P. Bauer, and F. J. Turk, Eds., 2007: *Measuring Precipitation from Space: EURAINSAT and the Future*. Advances in Global Change Research, Vol. 28, Springer, 722 pp.
- Machado, L. T., J. P. Duvel, and M. Desbois, 1993: Diurnal variations and modulation by easterly waves of the size distribution of convective cloud clusters over West Africa and the Atlantic Ocean. *Mon. Wea. Rev.*, **121**, 37–49.
- Mathon, V., H. Laurent, and T. Lebel, 2002: Mesoscale convective system rainfall in the Sahel. *J. Appl. Meteor.*, **41**, 1081–1092.
- Mohr, K. I., 2004: Interannual, monthly, and regional variability in the wet season diurnal cycle of precipitation in sub-Saharan Africa. *J. Climate*, **17**, 2441–2453.
- Morrissey, M. L., J. A. Maliekal, J. S. Greene, and J. Wang, 1995: The uncertainty of simple spatial averages using rain gauge networks. *Water Resour. Res.*, **31**, 2011–2017.
- Mounier, F., G. N. Kiladis, and S. Janicot, 2007: Analysis of the dominant mode of convectively coupled Kelvin waves in the West African monsoon. *J. Climate*, **20**, 1487–1503.
- Negri, A. J., E. J. Nelkin, R. F. Adler, G. J. Huffman, and C. Kummerow, 1995: Evaluation of passive microwave precipitation algorithms in wintertime midlatitude situations. *J. Atmos. Oceanic Technol.*, **12**, 20–32.
- Nesbitt, S. W., and E. J. Zipser, 2003: The diurnal cycle of rainfall and convective intensity according to three years of TRMM measurements. *J. Climate*, **16**, 1456–1475.
- , —, and C. D. Kummerow, 2004: An examination of version-5 rainfall estimates from the TRMM Microwave Imager, Precipitation Radar, and rain gauges on global, regional, and storm scales. *J. Appl. Meteor.*, **43**, 1016–1036.
- Nicholson, S. E., and Coauthors, 2003a: Validation of TRMM and other rainfall estimates with a high-density gauge dataset for West Africa. Part I: Validation of GPCC rainfall product and pre-TRMM satellite and blended products. *J. Appl. Meteor.*, **42**, 1337–1354.
- , and Coauthors, 2003b: Validation of TRMM and other rainfall estimates with a high-density gauge dataset for West Africa. Part II: Validation of TRMM rainfall products. *J. Appl. Meteor.*, **42**, 1355–1368.
- North, G. R., and S. Nakamoto, 1989: Formalism for comparing rain estimation designs. *J. Atmos. Oceanic Technol.*, **6**, 985–992.
- Pardo-Igúzquiza, E., D. I. F. Grimes, and C.-K. Teo, 2006: Assessing the uncertainty associated with intermittent rainfall fields. *Water Resour. Res.*, **42**, W01412, doi:10.1029/2004WR003740.
- Peyrillé, P., and J. P. Lafore, 2007: An idealized two-dimensional framework to study the West African monsoon. Part II: Large-scale advection and the diurnal cycle. *J. Atmos. Sci.*, **64**, 2783–2803.
- , —, and J.-L. Redelsperger, 2007: An idealized two-dimensional framework to study the West African monsoon. Part I: Validation and key controlling factors. *J. Atmos. Sci.*, **64**, 2765–2782.
- Redelsperger, J.-L., A. Diongue, A. Diedhiou, J. P. Ceron, M. Diop, J.-F. Gueremy, and J.-P. Lafore, 2002: Multi-scale description of a Sahelian synoptic weather system representative of the West African monsoon. *Quart. J. Roy. Meteor. Soc.*, **128**, 1229–1258.
- , C. D. Thorncroft, A. Diedhiou, T. Lebel, D. J. Parker, and J. Polcher, 2006: African Monsoon Multidisciplinary Analysis: An international research project and field campaign. *Bull. Amer. Meteor. Soc.*, **87**, 1739–1746.
- Roca, R., J.-P. Lafore, C. Piriou, and J.-L. Redelsperger, 2005: Extratropical dry-air intrusions into the West African monsoon midtroposphere: An important factor for the convective activity over Sahel. *J. Atmos. Sci.*, **62**, 390–407.
- , and Coauthors, 2010: On the water and energy cycles in the tropics. *C. R. Geosci.*, in press.
- Sapiano, M. R. P., and P. A. Arkin, 2009: An intercomparison and validation of high-resolution satellite precipitation estimates with 3-hourly gauge data. *J. Hydrometeorol.*, **10**, 149–166.
- Sultan, B., and S. Janicot, 2003: The West African monsoon dynamics. Part II: The “preonset” and “onset” of the summer monsoon. *J. Climate*, **16**, 3407–3427.
- , —, and A. Diedhiou, 2003: The west african monsoon dynamics. Part I: Documentation of intraseasonal variability. *J. Climate*, **16**, 3389–3406.
- Teo, C.-K., and D. I. F. Grimes, 2007: Stochastic modelling of rainfall from satellite data. *J. Hydrol.*, **346**, 33–50.
- Ushio, T., and Coauthors, 2009: A Kalman filter approach to the Global Satellite Mapping of Precipitation (GSMaP) from combined passive microwave and infrared radiometric data. *J. Meteor. Soc. Japan*, **87A**, 137–151.
- Viltard, N., C. Burlaud, and C. D. Kummerow, 2006: Rain retrieval from TMI brightness temperature measurements using a TRMM PR-based database. *J. Appl. Meteor. Climatol.*, **45**, 455–466.
- Xie, P., A. Yatagai, M. Chen, T. Hayasaka, Y. Fukushima, C. Liu, and S. Yang, 2007: A gauge-based analysis of daily precipitation over East Asia. *J. Hydrometeorol.*, **8**, 607–626.
- Yang, S., and E. A. Smith, 2006: Mechanisms for diurnal variability of global tropical rainfall observed from TRMM. *J. Climate*, **19**, 5190–5226.
- Zeweldi, D. A., and M. Gebremichael, 2009: Sub-daily scale validation of satellite-based high-resolution rainfall products. *Atmos. Res.*, **92**, 427–433, doi:10.1016/j.atmosres.2009.01.001.